11th AIAA/CEAS Aeroacoustics Conference (26th AIAA Aeroacoustics Conference)
23 - 25 May 2005, Monterey, California

AIAA 2005-3093

Modeling Jet Noise from Organized Structures using Near-Field Hydrodynamic Pressure

R. Reba* and S. Narayanan†
United Technologies Research Center, E. Hartford, CT
T. Colonius‡
California Institute of Technology, Pasadena, CA
T. Suzuki§
University of Fukui, Fukui, Japan

A wave-packet ansatz is used to model noise generation by organized, large-scale structures. The spectrum of the acoustic field is expressed in terms of two-point space-time correlations of hydrodynamic pressure on a conical surface surrounding the jet plume. The surface is sufficiently near the turbulent flow region to be dominated by hydrodynamic disturbances, yet sufficiently far that the wave equation can be used to project the near-field pressure to the acoustic field. In the present study, a 78-microphone array was used to measure hydrodynamic pressure on the conical surface at a variety of acoustic Mach numbers and temperature ratios. At each jet cross section, 6 microphones are staggered in the azimuthal direction allowing resolution of pressure up to azimuthal mode number m=2. We compare recent jet noise measurements using an 80-microphone conical mid-field array with those derived from the near-field hydrodynamic array data, showing reasonably good predictions. Source model parameters are identified for various jet temperature ratios. Results show that changes in jet noise directivity with heating can be attributed to contraction of the wave-packet scale.

I. Introduction

The generation of noise from high-speed, turbulent jets is of significant practical interest (e.g., for subsonic civil transport), receiving widespread attention for decades. The need to reduce aircraft exhaust noise in the face of increasingly stringent environmental regulations has led to numerous studies aimed at understanding the underlying noise sources and developing means to mitigate them. Numerous experimental and analytical approaches to explore the connection between shear flow turbulence and noise have been pursued since the pioneering work of Lighthill,[1] some of which are described below.

Tam et al.[2] reported that measured far-field noise spectra from single stream jets can be described by a pair of characteristic spectral shapes, having distinct directivity, that were associated with fine and large-scale turbulence structures. Noise generation associated with the former mechanism (hypothesized to be due to fine-scale turbulence) has received significant attention resulting in semi-empirical models (relating two-point turbulence statistics to noise) coupled to RANS computations (reviewed by Tam[3]). On the other hand, much less in the way of analytical models or computations exist concerning jet noise generation due to large-scale structures. Large-eddy simulations[4,5] for jet noise are only now becoming feasible at moderate Reynolds numbers, and use of reduced-order models[6,7] to explore noise generation from unsteady, organized aspects of turbulence (such as large-scale vortices and their interactions) is still in its infancy.

The preferential amplification of disturbances in certain frequency bands leads to the formation, interaction and subsequent decay of organized instabilities and vortical structures in free shear flows such as the jet.[8]

*Senior Research Engineer, Acoustics, AIAA Member.
†Project Leader, Pratt and Whitney Program Office, AIAA Member.
‡Associate Professor of Mechanical Engineering, AIAA Member.
§Assistant Professor, Graduate School of Engineering.

Copyright © 2005 by the author(s). Published by the American Institute of Aeronautics and Astronautics, Inc., with permission.

One might therefore describe the acoustic behavior of the jet in terms of the growth and decay of a coherent structure. This notion parallels the association of sound generation with linear instability waves invoked by past researchers.[9,10] For very low Mach number flows, Crighton and co-workers elucidated the superdirective nature of noise radiation and its dependence on the (wave amplitude) envelope shape (inferred from Laufer and Yen[11] measurements of near-field pressure in a jet) and size (relative to the acoustic wavelength). Morris and Tam[12] computed far field sound from linear instability waves for highly supersonic jet flows, where a supersonic convective wave speed (relative to the ambient sound speed) enables efficient coupling with the acoustic field. More recently, analysis of nonlinear evolution of supersonic instability waves has also been performed for $M > 2$.[13] However, such analytical treatment becomes limited and computationally cumbersome in high subsonic jets, where only a small portion of the frequency-wavenumber distribution of the relevant scales of motion extend to the radiating supersonic region.[14]

Several experimental approaches to inferring the sound sources using in-flow velocity and near/far-field pressure measurements have been proposed over the years. Some of the earliest measurements of pressure fluctuations due to coherent structures and their connection with jet noise radiation were reported by Mollo-Christensen.[15] In-flow measurements of density and velocity fluctuations simultaneously with far field noise measurements have also been reported,[16–18] aiming to establish a direct cause-and-effect relationship between turbulence characteristics and far field noise. Motivated by the measurements of pressure correlations in the jet (such as by Fuchs[19]), Michalke[20] analytically investigated the effect of the spatial extent of the source coherence on noise generation. It was shown that for jets with convection Mach number near unity, larger and more 'focused' noise radiation in the aft angles occurs with increasing source coherence (relative to a length scale based on the source volume). More recently, non-intrusive means to the causality approach have been pursued,[21] but remain limited to pointwise measurements. Such measurements describe local turbulence characteristics well but are ineffective in capturing flow motions over spatially extended regions. Consequently, local flow quantities will correlate weakly with far field sound and be limited to only the low frequencies for which the sources are coherent over a large flow region. Zaman[22] examined the near and far field pressure of a subsonic jet, attempting to describe noise sources in terms of the overall turbulence characteristics, without establishing direct correlations with organized flow structures. Ukeiley and Ponton[23] characterized the dynamic and three-dimensional nature of hydrodynamic pressure signatures over a spatially extended jet region and speculated the connection between lower azimuthal mode number structures at low frequencies and the far-field noise. Recent studies,[24,25] have also attempted to relate (albeit qualitatively) the dynamics of large-scale structures within the jet shear layers to the far field sound generation at low frequencies and in the aft angles. The origin of sound waves were inferred from the phase lag between individual microphones of a small array of far field microphones. Coupled with simultaneous (scalar) visualizations of the flow field, insights into the evolution of flow structures and the peak noise generation were obtained. However, a more robust and quantitative approach to verifying the role of the large-scale flow structures to the far-field sound is still lacking. In particular, none of the aforementioned measurements have been used to (quantitatvely) project sound levels in the far field.

In summary, the quantitative relationship between organized structures in a jet flow and the far field noise generation has not been satisfactorily addressed. Particularly lacking is a parametric modeling framework enabling a better understanding of the sensitivity of the acoustic field to changes in the flow structure evolution. This would facilitate the development of innovative and effective jet noise reduction concepts. The present study is directed at providing such a modeling framework.

The modeling described herein relies on a wave-packet based description of near-field pressure on a conical surface in the linear, hydrodynamic region of the jet. Thus, the source is described by second order statistics of a scalar quantity over a surface, in contrast with the Lighthill Analogy approach requiring fourth-order statistics of a vector quantity over a volume. Although the source description adopted here is less fundamental than that of Lighthill, it can be measured experimentally with relative ease.

The present study is an extension of exploratory work[27] where a simple three-microphone technique was used. Here we utilize near-field array data acquired by Suzuki and Colonius[26] in partnership with NASA Glenn Research Center. A large microphone array was used to simultaneously measure pressure time traces over a substantial axial extent surrounding the jet and with adequate axial and circumferential resolution.

II. Experimental Facility and Method

We briefly describe salient details of the experimental facilities; further details regarding the microphone array measurements are given in Suzuki & Colonius[26] and particle image velocimetry (PIV) and other flow measurements are discussed by Bridges & Wernet[29] and Bridges & Brown.[28] The experiments were conducted using the Small Hot Jet Acoustic Rig (SHJAR) at NASA Glenn Research Center. A single-stream round jet issued from a converging nozzle with 2 in. exit diameter. The nozzle was mounted 3.05m from the ground in an anechoic dome with a 20m radius. Straight and chevron nozzles were tested but the present discussion is limited to results from the straight nozzle. Experiments were conducted at a variety of set points from the matrix of Tanna.[30] PIV measurements were previously made in in-flow and cross-flow planes for each of the operating conditions.[28,29] Averaged PIV data was used by Suzuki & Colonius[26] to construct linear instability eigenfunctions that were used in processing the microphone array data with a beam-forming technique in order to detect the amplitude and streamwise variation of instability waves, as described in greater detail in IV.

Microphones were placed in two conical array configurations depicted in figure 1. In the first case (figure 1a), a 78 microphone array was placed just outside the jet mixing layers in order to measure the hydrodynamic pressure associated with large-scale turbulent structures (instability waves). The array location and microphone spacing were designed by Suzuki & Colonius[26] based on linear stability analysis of the jet mean flow fields (from PIV) in order to detect instability waves over a range of low frequencies and azimuthal mode numbers from 0 (axisymmetric) to 2. The array has 13 rings with $0.625D$ inter-ring spacing and a total axial extent just over $8D$. Six microphones are placed on each ring with an equal spacing of 60°; microphones are staggered in the azimuthal direction by an amount of 30° at every other ring. The spacing and axial positions were determined to allow just 7 rings of microphones to span approximately two wavelengths of the instability waves at the peak frequency for the beam-forming detection algorithms. The spreading angle of the array (cone half angle) is 11.3°, determined to be slightly wider than the spreading of the velocity fluctuations. The entire array could be shifted along the jet axis; six axial positions of the array were tested. The error in microphone position was estimated to be less than $0.05D$ from a noise-source test using a spark plug. This error is at most 5% of the instability wavelength. The background noise amplitude was at least three orders of magnitude smaller than signals from the jet.

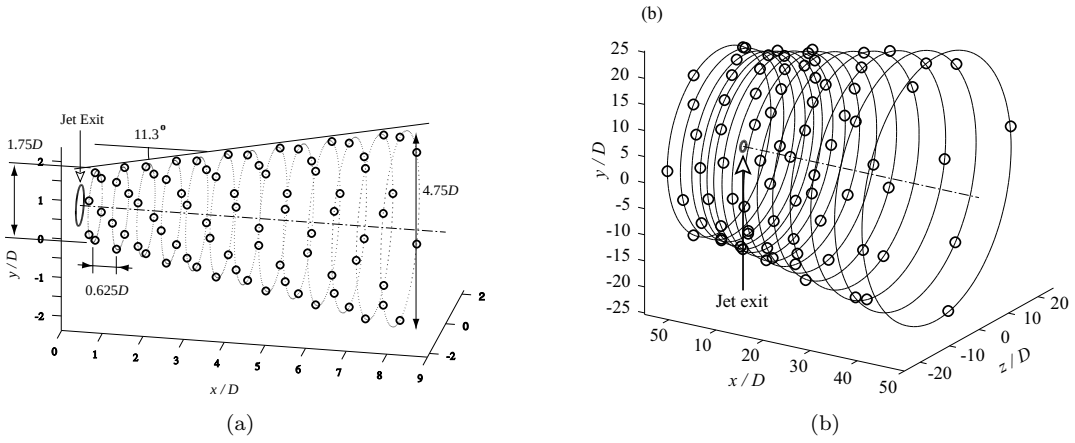

Figure 1. Microphone distributions of (a) near-field hydrodynamic array and (b) mid-field acoustic array.

The second array (figure 1b) was designed by James Bridges (NASA Glenn) to measure the acoustic field. In what follows we refer to this as the mid-field array since microphones were placed in the range of $17.3D < r < 25D$, which is about 2 to 3 wavelengths of sound at the peak frequency. The array covers zenithal angles in the acoustic field (measured from the downstream direction) of 31.7° to 106.3°. Fifteen axial ring positions were designed to give nearly equally spaced zenithal angles. The 10 rings furthest upstream have 6 microphones per ring (equally spaced in the azimuthal direction and staggered from ring to ring, while the 5 rings furthest downstream have 4 microphones per ring. Errors in microphone positions are less than $0.1D$ based on photographic analysis.

III. Analysis

A. Acoustic projection method

The objective of the current study is to sense the pressure signatures of large-scale turbulent structures in the jet near field, and analytically relate their statistical properties to sound radiation. Toward this end, we assume that the near-field microphones are in a region where pressure is governed by the linear wave equation. Thus, we require that the measurement location is sufficiently *near* the jet such that the pressure field is dominated by hydrodynamic disturbances, yet sufficiently *far* from the jet such that the effects of non-linearity and mean flow non-uniformity can be reasonably neglected.

We solve the wave equation

$$\partial^2 p/\partial t^2 - c_0^2 \partial^2 p/\partial x_i^2 = 0 \tag{1}$$

with pressure specified on a cylindrical surface of radius $r = r_0$ encompassing the jet. This is a simplifying approximation to the conical surface on which pressure data is acquired. Equation (1) is solved by applying Fourier transforms in the streamwise (x) and azimuthal directions (θ), and solving the resulting boundary value problem in the radial coordinate with boundary condition specified at $r = r_0$. A disadvantage of this approach is the need to specify pressure data along the entire x axis, while the near-field array data extends only 7 to 9 jet diameters downstream of the nozzle exit. However, this approach admits straightforward analytical solutions, and was preferred for the feasibility assessment presented here. Future efforts will include alternative treatments of the downstream region, as well as exact accounting for the conical array geometry.

In discussing the analytical solution, we take $x = 0$ to coincide with the last microphone position in the array, so that the nozzle exit is at some $x < 0$. In the downstream region $x > 0$ we apply the impermeable-wall boundary condition

$$\frac{\partial p}{\partial r}(x > 0, r_0, \omega) = 0. \tag{2}$$

Thus, grazing rays along the jet axis experience an artificial solid-wall boundary condition, and processing of these rays by the mean flow of the downstream jet plume is neglected. This boundary condition was preferred to the perhaps more obvious approach of setting $p = 0$ for $x > 0$; in this case, the downstream region acts as sound-absorbing (pressure-release) surface, causing significant attenuation of the sound field in the aft-most angles.

The pressure field can be expressed as

$$p_m(x, r; \omega) = \frac{1}{2\pi} \int_{-\infty}^{\infty} \hat{p}_m(\delta, r_0; \omega) F_m(x, r; \delta, \omega) d\delta \tag{3}$$

where

$$\hat{p}_m(\delta, r_0; \omega) = \int_{-\infty}^{0} p_m(x, r_0; \omega) e^{\mathrm{i}\delta x} dx \tag{4}$$

and F_m is the fundamental solution satisfying (1) and (2)along with

$$F_m(x < 0, r_0; \delta, \omega) = \mathrm{e}^{-\mathrm{i}\delta x}. \tag{5}$$

The mixed boundary value problem for F_m is solved using the Wiener-Hopf technique.

The jet pressure spectral density at azimuthal mode m can then be expressed as

$$P_m(x, r, \omega) = \frac{1}{4\pi^2} \int R_m(\xi', \xi, r_0, \omega) F_m^*(x, r; \delta, \omega) F_m(x, r; \delta', \omega') \mathrm{e}^{-\mathrm{i}\delta\xi} \mathrm{e}^{\mathrm{i}\delta'\xi'} d\delta d\delta' d\xi d\xi' \tag{6}$$

where

$$R_m(\xi', \xi, r_0, \omega) \equiv \int \langle p_m^*(\xi, r_0, t) p_m(\xi', r_0, t + \tau) \rangle \, \mathrm{e}^{\mathrm{i}\omega\tau} d\tau \tag{7}$$

is the pressure cross-spectral matrix on the near-field surface $r = r_0$. Previously[27] the four-fold integration in (6) was simplified by invoking far-field approximations. An alternative simplifying step, not restricted to the acoustic far field, is to apply Proper Orthogonal Decomposition, whereby the correlation function can be written

$$R_m(\xi', \xi, r_0, \omega) = \sum_n \lambda^{(n)} \phi_m^{(n)}(\xi', r_0, \omega) \phi_m^{(n)*}(\xi, r_0, \omega) \tag{8}$$

where $\phi^{(n)}$are eigenfunctions of the correlation function, and $\lambda^{(n)}$ are the corresponding eigenvalues. The jet pressure spectral density is then given by

$$P_m(x,r,\omega) = \sum_n \lambda^{(n)} \left| \frac{1}{2\pi} \int_{-\infty}^{\infty} \hat{\phi}_m^{(n)}(\delta, r_0, \omega) F_m(x,r;\delta,\omega) d\delta \right|^2 . \tag{9}$$

For the numerical results presented here, all modes were retained in the above summation.

B. Analytical source model

In the present formulation, the pressure cross-spectrum R_m constitutes the acoustic source. In the following, we estimate this source from near-field array data, and use the result to reconstruct the acoustic field. The amplitude and real part of R_m are shown in figure 2 at $St = 0.2$ for a heated jet with acoustic Mach number 0.9. The pressure cross-spectrum takes the form of an amplitude-modulated traveling wave with peak amplitude at $x/D \cong 4.5$. Phase iso-contours are seen to diverge with downstream distance, corresponding to decreasing wavenumber, and increasing phase speed. We consider a model for R_m in the form of a modified wave-packet

$$R_m(x',x,r_0,\omega) = A(x-a)(x'-a) \exp\left[-\frac{(\bar{x}-b)^2}{L_1^2} - \frac{(\Delta x)^2}{L_2^2} \right] \mathrm{e}^{\mathrm{i}k(\bar{x})\Delta x} \tag{10}$$

where $\bar{x} = (x+x')/2$, $\Delta x = (x-x')/2$, and

$$k(\bar{x}) = c\bar{x} + d. \tag{11}$$

Note that the coordinates $\bar{x}$ and Δx correspond to the mean microphone location, and microphone half-separation, respectively. The length scale L_1 characterizes the streamwise extent of the active source region, and L_2 characterizes the streamwise correlation scale. Thus, a wave-packet with $L_1 \gg L_2$ represents a broad distribution of locally correlated pressure. Conversely, for a wave-packet with L_1 on the order of L_2, pressure is correlated over a scale comparable to the source region.

The above model for R_m provides a good fit to the data, as shown in figure 2c. Identification of source model parameters is discussed further in IV.

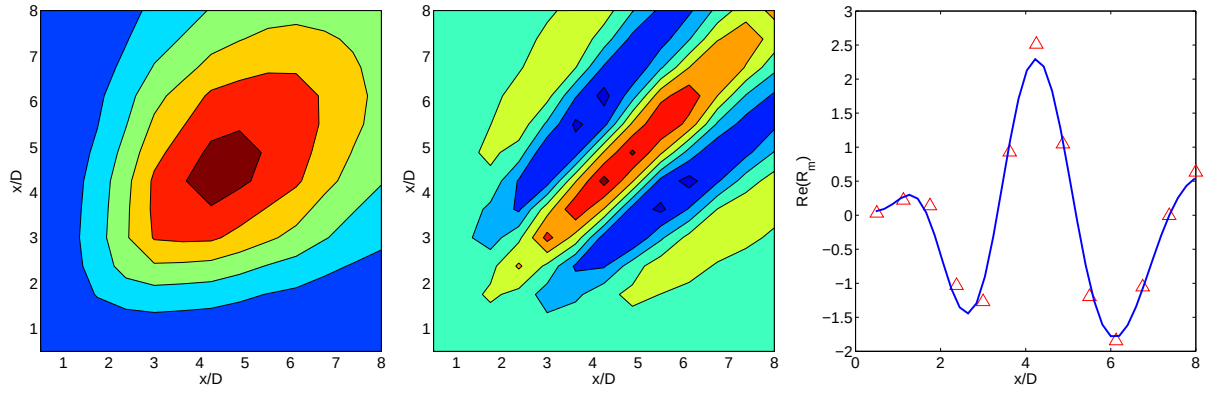

(a) (b) (c)

Figure 2. (a) Amplitude and (b) real part of R_m for sp27, m=0. (c) Model function compared to data for real part of R_m at $x/D \simeq 4.5$.

IV. Results and Discussion

A. Near-field pressure analysis

We briefly review some previous data analysis[26] for the near-field array. In this work, the beam-forming algorithm was adapted to detect the signatures of instability waves convecting in the jet mixing layers.

Essentially, the monopole source used as the kernel in standard beam-forming techniques was replaced with eigenfunctions from (weakly nonparallel) linear stability analysis of the experimentally measured jet mean velocity field. The output of the algorithm is the overall amplitude of the eigenfunction that best matches (in a least-squared sense) the measured signal. The algorithm attempts to minimize any contributions to the observed signals from uncorrelated events (e.g. contributions from convecting smaller-scale turbulence at the same frequency, or from acoustic waves at the same frequency). The results demonstrated that in a statistical sense, the eigenfunctions obtained from linear stability analysis well represent the coherent flow structures from the nozzle exit to the end of the potential core, particularly near the most amplified frequency of each azimuthal mode.

We can infer from these results that at the low frequencies of interest, the pressure measured along the near-field array is primarily composed of hydrodynamic (instability wave) pressure fluctuations rather than acoustic radiation. This is important in assessing the viability of the far-field projection method developed in the present paper, since the goal is to devise a model that establishes the transfer function between coherent large-scale structures and the far-field sound (not merely to project the sound from one location to another). To demonstrate that this is the case, figure 3 compares pressure measured along the near-field array with eigenfunctions from linear stability analysis whose amplitude has been determined by the aforementioned beam-forming technique. For the data presented in the figure, we take Fourier transforms in the azimuthal direction and in time of the 6 microphones on any given ring (we call this the *ring-wise* pressure). Note that here only 7 streamwise rings are plotted since this was the subset of microphones used in the beam-forming technique. There is in general a good agreement between the ring-wise data and the eigenfunctions. Previous analysis[26] has also shown that pressure at each axial station of the array follows exponential (rather than algebraic) decay with radius, consistent with being in the hydrodynamic near-field (see figure 3a). For sufficiently large radii, algebraic decay, indicative of acoustic behavior, is found.

To further demonstrate that hydrodynamic events are recorded by the near-field array, figures 4a,b show the phase of R_0 at $St = 0.2$ at an acoustic Mach number of 0.9, and temperature ratios of 1.76 and 2.7 (set points 27, 46 from Table 1). The steeper trend line corresponds to a phase speed of $0.7U_j$, and the shallow line corresponds to the phase speed of an acoustic wave propagating along the jet axis. Phase speeds increase with downstream distance, presumably due to increasing contribution from acoustics. We can see, however, that the dominant phase behavior at the peak of the wave-packet is indicative of hydrodynamics.

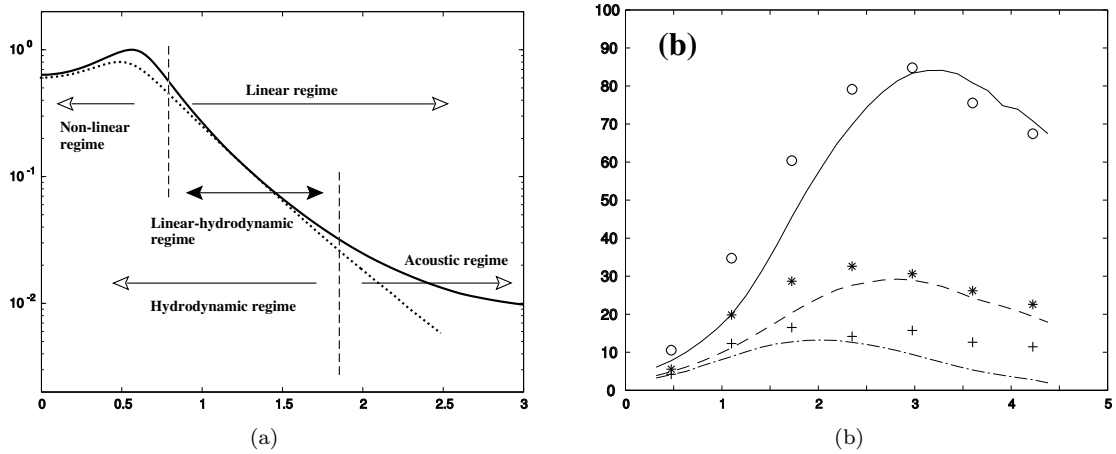

Figure 3. (a) Schematic of flow regimes as function of radial distance r/D_j from jet centerline. (b) Comparison of pressure at $St = 0.3$ measured along near-field array and eigenfunctions from linear stability whose amplitude is determined by the beam-forming algorithm.[26] $M_\infty = 0.9$ and $T_j/T_\infty = 2.7$. Solid lines are eigenfunctions: ——, $m = 0$; − − −, $m = 1$; − · − · −, $m = 2$. The symbols are ring-wise pressure amplitude: ∘, $m = 0$; ∗, $m = 1$; +, $m = 2$.

B. Acoustic projection

In this section we compare acoustic measurements along the mid-field array with those projected from the near-field hydrodynamic data. Results are presented for the jet operating conditions in Table 1. Set points

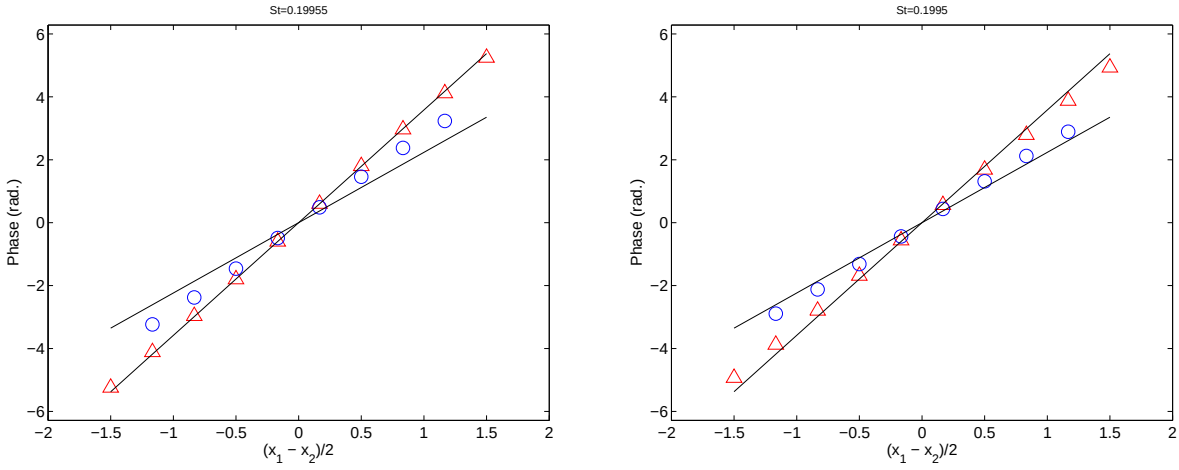

(a) sp27 (b) sp46

Figure 4. Phase of R_0 at peak amplitude (triangles) and 2.5 diameters downstream of peak (circles);$St = 0.2$. Steep line corresponds to phase speed of $0.7U_j$. Shallow line corresponds to sonic phase speed.

7, 27, and 46 are at a fixed acoustic Mach number of 0.9 with temperature ratios of 0.84, 1.76 and 2.7, respectively. Set points 23, 27, and 29 are at a fixed temperature ratio of 1.76, with acoustic Mach numbers of 0.5, 0.9 and 1.33, respectively.

As discussed above, the projection method assumes boundary data is specified on a cylindrical surface of radius $r = r_0$, whereas the near-field array has a spreading angle of 11.3°. In the following results, we take $r_0 = 1.65D_j$, corresponding to the mean array radius. Sensitivity to the choice of r_0 is approximately $\mp 1.5dB$ for r_0 in the range of $0.9D_j$ to $2.4D_j$, corresponding to the minimum, and maximum radii of the near-field array, respectively.

Set pt.	M_∞ (M_{jet})	T_{jet}/T_∞	Re
7	0.90 (0.98)	0.84 (cold)	16×10^5
23	0.50 (0.38)	1.76 (hot)	2×10^5
27	0.90 (0.69)	1.76 (hot)	4×10^5
29	1.33 (0.98)	1.76 (hot)	6×10^5
46	0.90 (0.56)	2.70 (hot)	2×10^5

Table 1. Operating conditions of jet flows. $M_{\text{jet}} \equiv (U/a)_{\text{jet}}$ and Re $\equiv (\rho UD/\mu)_{\text{jet}}$.

We first present results for azimuthal mode m=0. Comparisons of projected and measured sound pressure are presented in figures 5 and 7 at constant acoustic Mach number, and constant temperature ratio, respectively. Sound pressure levels are shown as a function of polar angle along the mid-field array for Strouhal numbers of 0.2 and 0.4. Projected pressure levels are in good agreement with mid-field array data for polar angles above 50°. At lower angles, levels are consistently under-predicted, with the largest error of approximately 10dB observed for set points 7 and 29. Conversely, the low-angle discrepancy is smallest for the heated set point 46 at acoustic Mach 0.9, and heated set point 23 at acoustic Mach number 0.5.

Corresponding wave-packet amplitudes are shown in figures 6 and 8 at constant acoustic Mach number, and constant temperature ratio, respectively. At each frequency, agreement between measured and projected levels improves as the peak of the wave-packet moves upstream, and more of the active source region is encompassed by the array. This trend suggests that errors in the projection are associated with insufficient downstream extent of the array.

We next present results for azimuthal mode $m = 1$. Comparisons of projected and measured sound pressure at constant temperature ratio are presented in figure 9. We note that radiation at mode $m = 1$ tends to be less aft-directive as compared to $m = 0$. As in the comparisons for $m = 0$, agreement between

measured and projected levels improves as the peak of the wave-packet moves upstream. In particular, the comparison at set point 23 is very good. In contrast with results for $m = 0$, however, the discrepancies are not restricted to the aft-most angles.

The above results for $m = 0$ and $m = 1$ suggest that errors in the projection are associated with insufficient downstream extent of the array. There are several related effects of insufficient array length, and the data are not consistent with a single explanation. It is conceivable that there is significant radiation from the active source region to shallow angles, especially toward the end of the array, which does not cross the array. Radiation at these extreme shallow angles would tend to be refracted by the jet plume, and perhaps account for the observed discrepancies around the peak angle at $m = 0$. However, this fails to explain observed trends at $m = 1$, where the discrepancies are not restricted to shallow angles.

Arguably, an additional source of error is the non-physical boundary condition applied on $r = r_0$ downstream of the array. Grazing rays along the jet axis experience an artificial solid wall boundary condition, whereas the physical acoustic field undergoes some interaction with the diverging jet plume.

Finally, figure 11 compares measured and projected sound pressure spectra at polar angles $\phi = 30°, 50°, 60°$ for set points 27, 46 and 29. Overall, trends in spectral shape, particularly spectral broadening with increasing angle, are captured. Also, the peak frequency tends to be captured in the aft-most angle. At higher angles, significant low frequency ($St < 0.2$) contamination obscures the spectral peak. This spurious noise source is the result of abrupt truncation of the wave-packet, which for $St < 0.2$ tends to peak near the boundary of the hydrodynamic array.

C. Source model parameter identification

Parameters in the source model (10) were identified by a least-squares fit to the measured cross-spectra R_m for set points 7, 27, and 46 at $St = 0.2$ and azimuthal mode $m = 0$. This series of set points is at a constant acoustic Mach number of 0.9, with varying temperature ratio (Table 1). Convection speeds are found to be comparable in all three cases (see figure 4 for comparison of set points 27 and 46). Length scales L_1 and L_2 are summarized in Table 2. The streamwise correlation scale L_2 shows little variation with temperature ratio. Length scale L_1, which characterizes the streamwise extent of the active source region, decreases with increasing temperature; this is presumably associated with shortening of the potential core. Thus, as temperature increases, the normalized correlation scale L_2/L_1 increases, and coherent dynamics account for a relatively larger portion of the active source region.

As jet temperature increases at fixed acoustic Mach number, we observe a broadening of the directivity pattern at mode $m = 0$ (figures 5 and 12a). In particular, there is a marked increase in radiation to moderate angles. Figure 12b illustrates sensitivity of the acoustic field to L_1 as computed from the R_m source model. L_1 was decreased by a factor of 0.8 from the baseline value identified for set point 27; other parameters (e.g. phases) were held constant, with the exception of amplitude A, selected to match set point 27 levels at 80°. Directivity patterns computed from the source model exhibit broadening similar to that seen in the data. These preliminary results suggest that contraction of the wave-packet scale L_1, namely shortening of the active source region relative to the correlation scale, is the controlling parameter for directivity broadening with increasing temperature.

Ongoing studies will further investigate influences of the wave-packet parameters on directivity, and other features of the acoustic field.

Set pt.	L_1	L_2	L_2/L_1
7	6.08	2.10	0.35
27	4.68	2.08	0.44
46	3.92	2.10	0.54

Table 2. Wave-packet length scales in units of D_j.

V. Conclusions

An analysis framework has been presented to describe noise generation by large-scale organized structures in jets. The approach attempts to relate statistics of near-field hydrodynamic pressure to far-field sound by

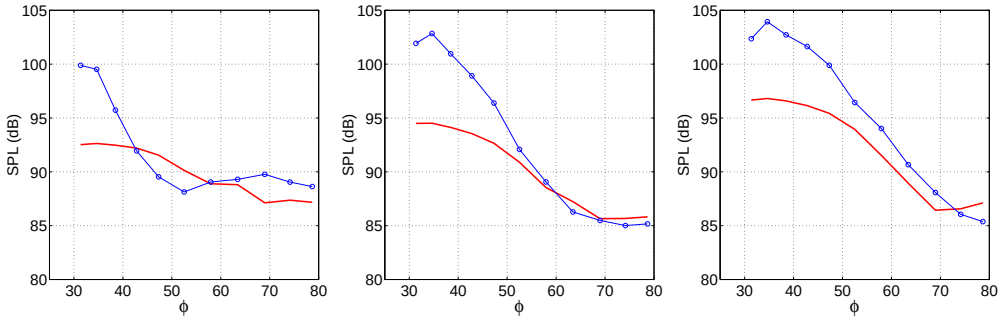

(a) sp7;St=0.2 (b) sp27;St=0.2 (c) sp46;St=0.2

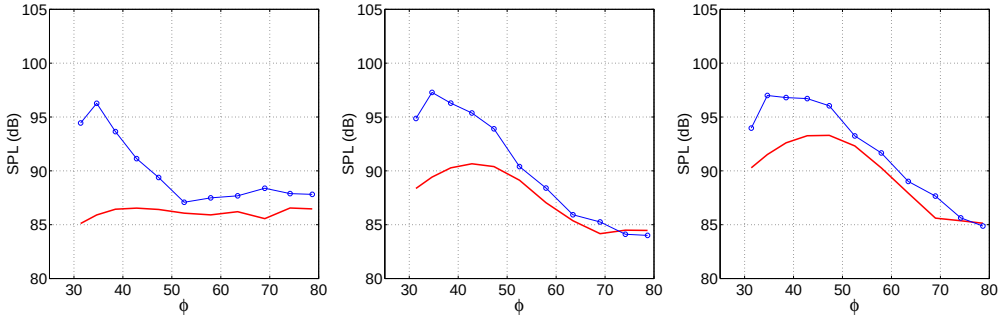

(d) sp7;St=0.4 (e) sp27;St=0.4 (f) sp46;St=0.4

Figure 5. Comparison of measured (symbols) and projected (solid red) sound pressure along mid-field array at $M_\infty = 0.9$; T_j increasing left to right. Set points 7, 27, 46 at $St = 0.2, 0.4; m = 0$.

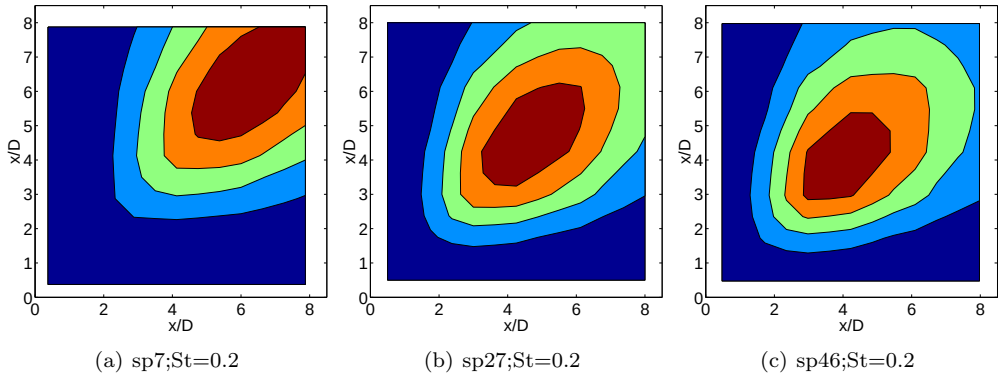

(a) sp7;St=0.2 (b) sp27;St=0.2 (c) sp46;St=0.2

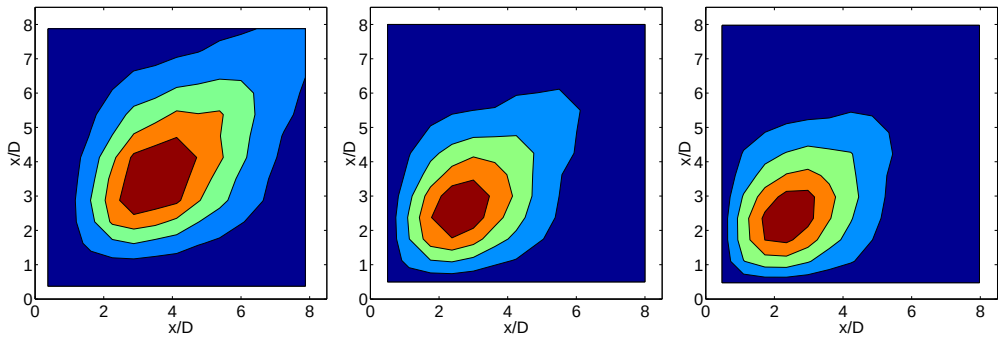

(d) sp7;St=0.4 (e) sp27;St=0.4 (f) sp46;St=0.4

Figure 6. Amplitude of R_m for set points 7, 27, and 46 at $St = 0.2, 0.4; m = 0$.

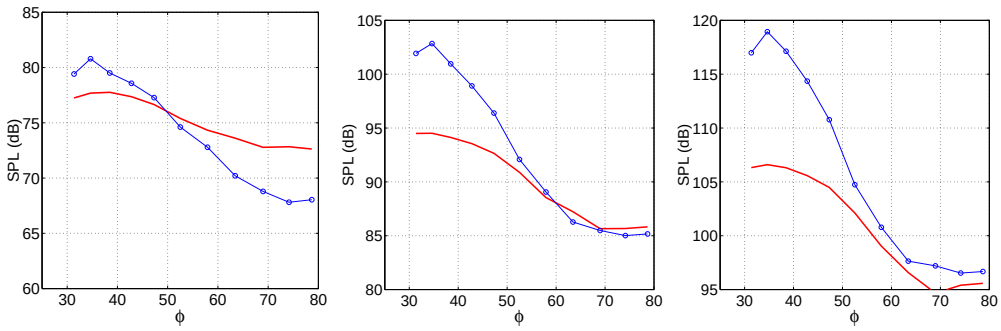

(a) sp23;St=0.2 (b) sp27;St=0.2 (c) sp29;St=0.2

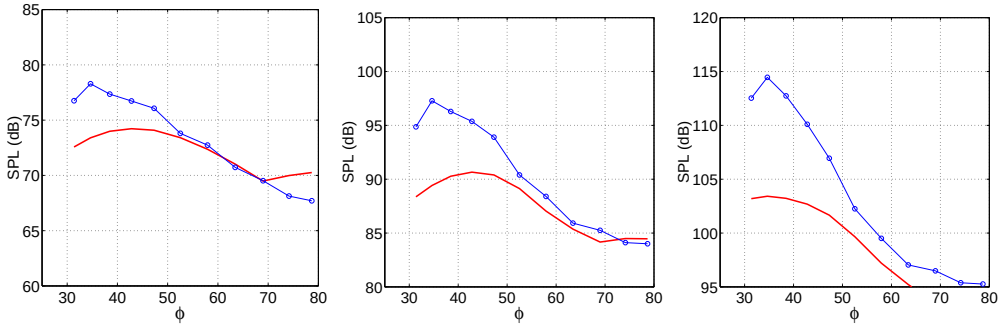

(d) sp23;St=0.4 (e) sp27;St=0.4 (f) sp29;St=0.4

Figure 7. Comparison of measured (symbols) and projected (solid red) sound pressure along mid-field array at $T_j/T_\infty = 1.76; M_\infty$ increasing left to right. Set points 23, 27, and 29 at $St = 0.2, 0.4; m = 0$.

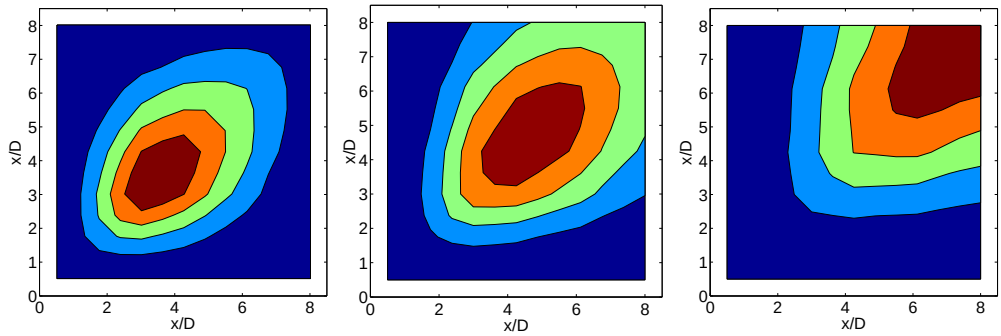

(a) sp23;St=0.2 (b) sp27;St=0.2 (c) sp29;St=0.2

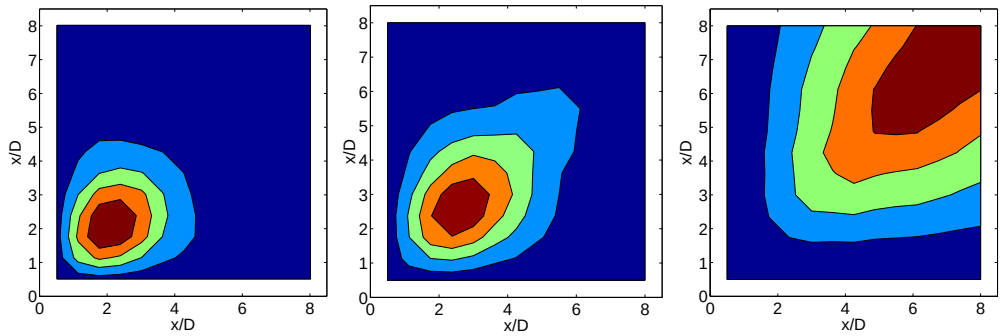

(d) sp23;St=0.4 (e) sp27;St=0.4 (f) sp29;St=0.4

Figure 8. Amplitude of R_m for set points 23,27, and 29 at $St = 0.2, 0.4; m = 0$.

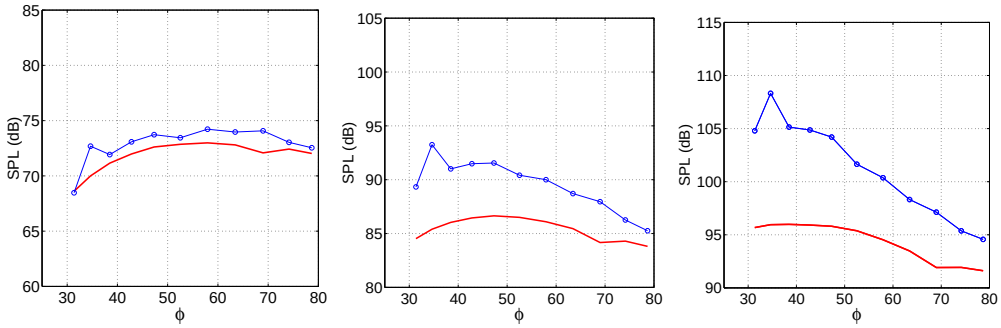

(a) sp23;St=0.2 (b) sp27;St=0.2 (c) sp29;St=0.2

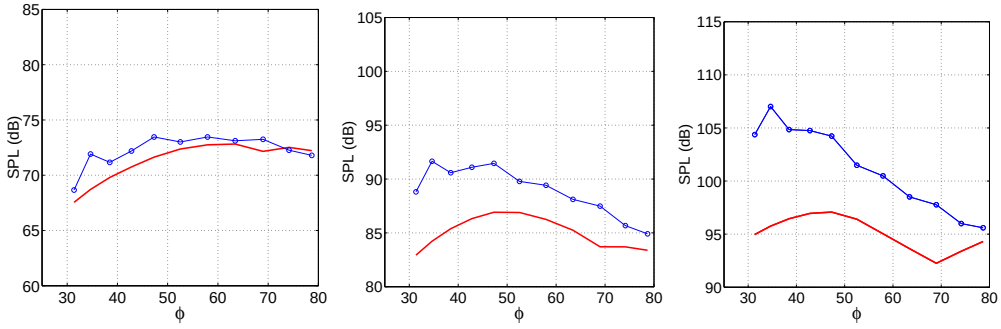

(d) sp23;St=0.4 (e) sp27;St=0.4 (f) sp29;St=0.4

Figure 9. Comparison of measured (symbols) and projected (solid red) sound pressure along mid-field array at $T_j/T_\infty = 1.76; M_\infty$ increasing left to right. Set points 23, 27, and 29 at $St = 0.2, 0.4; m = 1$.

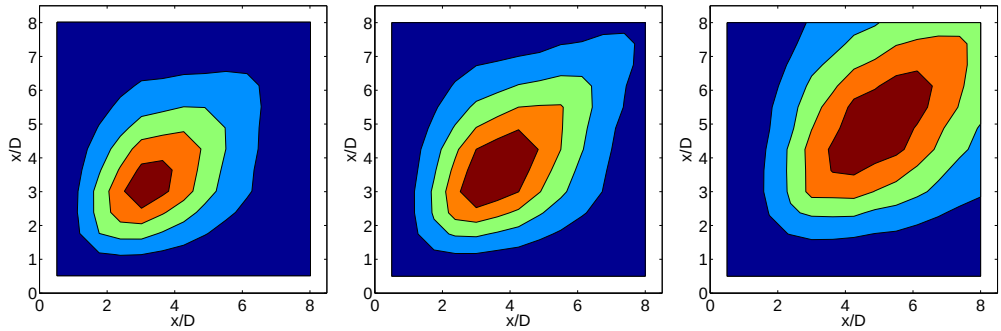

(a) sp23;St=0.2 (b) sp27;St=0.2 (c) sp29;St=0.2

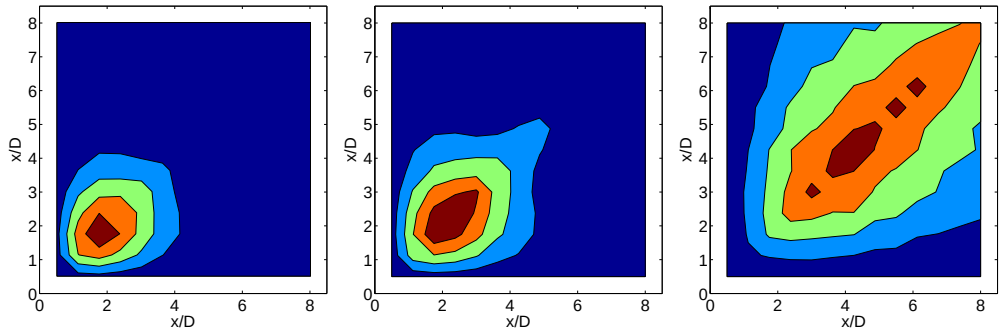

(d) sp23;St=0.4 (e) sp27;St=0.4 (f) sp29;St=0.4

Figure 10. Amplitude of R_m for set points 23,27, and 29 at $St = 0.2, 0.4; m = 1$.

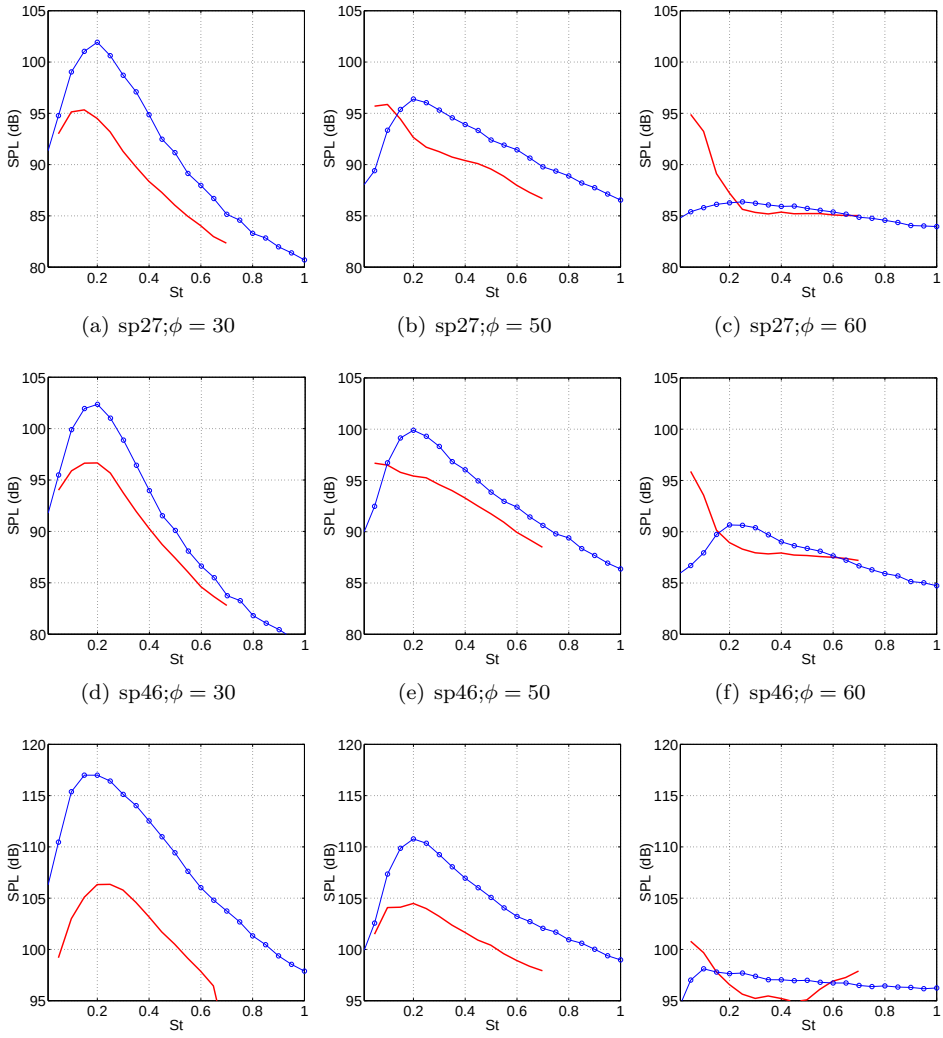

(a) sp27;$\phi = 30$ (b) sp27;$\phi = 50$ (c) sp27;$\phi = 60$

(d) sp46;$\phi = 30$ (e) sp46;$\phi = 50$ (f) sp46;$\phi = 60$

(g) sp29;$\phi = 30$ (h) sp29;$\phi = 50$ (i) sp29;$\phi = 60$

Figure 11. Comparison of measured (symbols) and projected (solid red) sound pressure spectra along mid-field array at polar angles $\phi = 30°, 50°, 60°$ for set points 27, 46 and 29; $m = 0$.

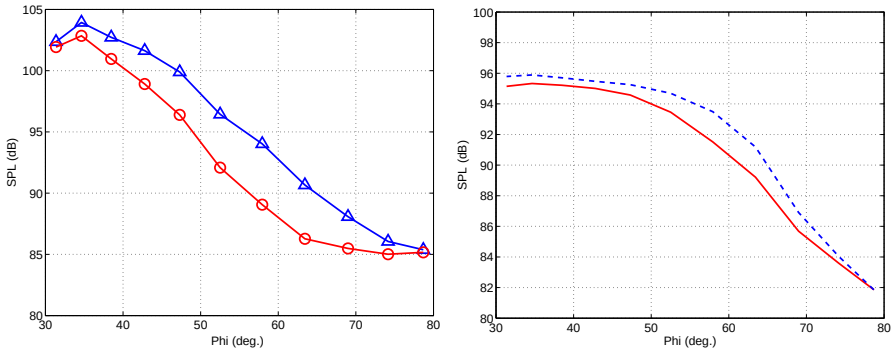

(a) (b)

Figure 12. (a) Comparison of measured sound pressure level along mid-field array for set points 27 (red circles) and 46 (blue triangles) at $St = 0.2, m = 0$. (b) Radiation at $St = 0.2, m = 0$ from wave-packet model based on set point 27 (solid red), and effect of reducing L_1 by factor of 0.8 (dashed blue).

applying the linear uniform-medium wave equation. We require, therefore, that the measurement location is sufficiently near the jet for signatures of hydrodynamic disturbances to be dominant, yet sufficiently far from the jet such that the effects of non-linearity and non-uniform mean flow can be neglected. This enables the projection of far-field noise due to coherent near-field structures, not a mere projection of sound from one location to another.

Results have demonstrated the feasibility of measuring pressure signatures of hydrodynamic disturbances, and relating their spatio-temporal statistics to sound generation. It is shown that, for low frequencies ($St < 0.4$), the near-field correlations are dominated by hydrodynamics. Acoustic pressure computed from the hydrodynamic data shows generally good agreement with far-field measurements. Trends in directivity, spectral shape and noise level are captured as a function of jet Mach number and temperature ratio. For $m = 0$, quantitative comparisons are good at polar angles above 50°. Discrepancies apparent at lower angles are the result of insufficient downstream extent of the array.

An analytical model has been developed for the measured hydrodynamic pressure correlations which constitute the acoustic source. An ansatz consisting of Gaussian wave packets is shown to provide a good approximation to the data. The resulting model characterizes the source in terms of a spatial scale, a spatial correlation scale, and a spatially non-uniform wavenumber. The parametric model has been used to investigate the effects of jet heating on directivity. Results show that broadening of the directivity pattern with heating can be attributed to contraction of the wave-packet envelope.

The semi-empirical modeling approach presented here offers a promising framework for analyzing sound generation from organized structures in a parametric fashion. This will aid in a better understanding of the sensitivity of the sound field to changes in the flow structure evolution. Such assessments will also be used to identify the distinguishing effects of jet noise reduction devices (e.g. tabs and chevrons) on the near field structure evolution and noise generation.

Acknowledgments

The authors are indebted to Drs. J. Bridges and S.-S. Lee for generously sharing their data and for fruitful discussions. TC and TS gratefully acknowledge the support of a grant from the Aeroacoustics Research Consortium (AARC) of the Ohio Aerospace Institute.

References

[1]Lighthill, M.J., "On sound generated aerodynamically I. General theory", Proc. Royal Soc., Vol. A221, pp.564-587, 1954.

[2]Tam, C.K.W., Golebiowski, M. & Seiner, J.M., "On the two components of turbulent mixing noise from supersonic jets," AIAA Paper 96-1716, 1996.

[3]Tam, C.K.W., "Jet Noise: Since 1952", Theor. Comp. Fluid Dynamics, Vol. 10, p. 393, 1998.

[4]Constantinescu, G.K. & Lele, S. K. "Large eddy simulation of a near sonic turbulent jet and its radiated noise," 39th Aerospace Sciences Meeting & Exhibit, January 8-11, Reno, NV, AIAA Paper-2000-0376, 2000.

[5]Bodony, D.J. & Lele, S.K., "Jet noise prediction of cold and hot subsonic jets using large-eddy simulation", AIAA Paper 2004-3022, 2004.

[6]Narayanan, S., Noack, B.R. & Meiburg, E., "Reduced order dynamical modeling of sound generation from a jet," 40th Aerospace Sciences Meeting & Exhibit, January 14-17, Reno, NV, AIAA Paper 2002-0073, 2002.

[7]Soteriou, M., Reba, R. & Maeder, T., "Numerical study of the impact of streamwise vorticity on noise generation by jet flows," 8th AIAA/CEAS Aeroacoustics Conference, June 17-19, Breckenridge, CO, AIAA Paper 2002-2480, 2002.

[8]Hussain, F., "Coherent structures and turbulence", J. Fluid Mech., Vol. , pp. , 1986.

[9]Huerre, P. & Crighton, D.G., "Sound generation by instability waves in a low Mach number jet", AIAA 8th Aeroacoustics Conference, April 11-13, Atlanta, GA, AIAA-83-0661, 1983.

[10]Crighton, D.G. & Huerre, P., "Shear-layer pressure fluctuations and superdirective acoustic sources", J. Fluid Mech., Vol. 220, pp. 355-368, 1990.

[11]Laufer, J. & Yen, T., "Noise generation by a low-Mach-number jet", J. Fluid Mech., Vol. 134, pp. 1-31, 1983.

[12]Morris, P.J. & Tam, C.K.W, "On the radiation of sound by instability waves of a compressible axisymmetric jet", in Mechanisms of Sound Generation in Flows (ed. E.A. Muller), Springer, 1979.

[13]Wu, X., "Mach wave radiation of nonlinearly evolving supersonic instability modes in shear layers", J. Fluid Mech., Vol. 523, pp. 121-159, 2005.

[14]Lin, R-S., Reba, R.A., Narayanan, S., Hariharan, N.S. & Bertolotti, F.P., "Parabolized stability equation based analysis of noise from an axisymmetric hot jet," Proceedings of ASME FEDSM-2004: High Speed Jet Flows, July 11-15, Charlotte, North Carolina, 2004.

[15]Mollo-Christensen, E., "Jet noise and shear flow instability seen from an experimenter's viewpoint", American Society of Mechanical Engineers Journal of Applied Mechanics, Vol. 89, pp. 1-7, 1967.

[16]Siddon, T.E., "Noise source diagnostics using causality correlations", AGARD CP 131, Noise Mechanisms, pp. 7-1:7-13, 1973.

[17]Seiner, J.M. & Reethof, G., "On the distribution of source coherency in subsonic jets", AIAA paper 74-4.

[18]Armstrong, R.R., Michalke, A. & Fuchs, H.V., "Coherent structures in jet turbulence and noise", AIAA J., Vol. 15(7), pp. 1011-1017, 1977.

[19]Fuchs, H.V., "Space correlations of the fluctuating pressure in subsonic turbulent jets", J. Sound and Vibration, Vol. 23, pp. 77-99, 1972.

[20]Michalke, A., "On the effect of spatial source coherence on the radiation of jet noise", J. Sound and Vibration, Vol. 55(3), pp. 377-394, 1977.

[21]Panda, J., Seashotlz, R.G. & Elam, K.A., "Measurement of correlation between flow density, velocity and density*velocity2 with far field noise in high speed jets", 8th AIAA/CEAS Aeroacoustics Coference, June 17-19, Breckenridge, CO, AIAA 2002-2485, 2002.

[22]Zaman, K.B.M.Q., "Flow field and near and far sound field of a subsonic jet", J. Sound and Vibration, Vol. 106(1), pp. 1-16, 1986.

[23]Ukeiley, L.S. & Ponton, M.K., "On the near field pressure of a transonic axisymmetric jet", Intl. J. of Aeroacoustics, Vol. 3(1), pp. 43-66, 2004.

[24]Hileman, J. & Samimy, M., "Turbulence structures and the acoustic far-field of a Mach 1.3 jet", AIAA J., Vol. 39(9), pp. 1716-1727, 2001.

[25]Hileman, J., Thurow, B. & Samimy, M., "Acoustic source localization using a 3-D microphones array in a Mach 1.3 jet", 40th Aerospace Sciences Meeting & Exhibit, January 14-17, Reno, NV, AIAA 2002-0366, 2002.

[26]Suzuki, T. & Colonius, T. "Identification of jet instability waves and design of a microphone array." AIAA Paper 2004-2960, 2004. Also submitted to *J. Fluid Mech.*

[27]Reba, R.A., Narayanan, S., Colonius, T. & Dunlop, M.J. "A study of the role of organized structures in jet noise generation", 9th AIAA/CEAS Aeroacoustics Conference and Exhibit, Hilton Head, SC, 2003, AIAA Paper 2003-3314.

[28]Bridges, J. & Wernet, M. "Measurements of the aeroacoustic sound source in hot jets." AIAA 2003-3130, 2003.

[29]Bridges, J. & Brown, C. "Parametric testing of chevrons on single flow hot jets." AIAA Paper 2004-2024, 2004.

[30]Tanna, H.K. "Experimental-study of jet noise: 1. Turbulent mixing noise." *J. Sound Vib.* Vol. 50(3), pp 405-428, 1977.